29.0 IDENTIFICATION OF DEFORMATION MECHANISMS OF THERMALLY STABLE CAST AL-CU ALLOYS VIA NEUTRON DIFFRACTION

Brian Milligan (CSM)
Faculty: Amy Clarke (CSM)
Industrial Mentor: Amit Shyam (Oak Ridge National Laboratory)

29.1 Project Overview and Industrial Relevance

29.1.1 Project Description

Cast Al-Cu alloys have long been popular in applications that require complex shapes, low density, and high strength. One such application is cylinder heads for internal combustion engines. However, as temperatures in commercial engines increase, the precipitates in these alloys begin to coarsen and transform during service. This leads to a loss of strength [29.1], due to a larger precipitate spacing [29.2], and a change in deformation mechanisms [29.3,29.4].

In order to fully understand and improve the mechanical properties, observing these properties from a grain perspective is required. This work includes neutron diffraction experiments, combined with synchrotron x-ray imaging and transmission electron microscopy (TEM) experiments, to understand the role of grain orientation and precipitate size/morphology on the mechanical properties.

29.1.2 Literature Review

Al-Cu precipitation has been studied in detail and generally follows the transformation pathway: supersaturated solid solution → plate-shaped, single atomic layer Guinier-Preston (GP) I zones → plate-shaped, 2-4 layer GPII/θ″ precipitates → thick, plate shaped θ′ precipitates → approximately spherical or rod-shaped θ equilibrium precipitates [29.2] Although precipitation behavior in Al-Cu alloys have been studied in detail, there is still room for investigation on the mechanisms of transformation, especially related to ternary and quaternary alloying elements. In particular, *in situ* methods including transmission electron microscopy [29.5] and 4-D (3-D plus time) transmission x-ray microscopy [29.6] are being implemented to study transformation phenomena, and have resulted in interesting observations regarding transformation mechanisms.

Yielding and strain hardening behavior in polycrystalline alloys have long been a popular area of study [29.7]. With modern computational tools and experimentation, models to describe these quantities are being continually refined. Of particular interest is the work of da Costa Teixiera *et al.*, who have removed the common assumption that precipitates are approximately spherical and have successfully improved the accuracy of predictive models of yielding and strain hardening in Al-Cu alloys [29.3, 29.4]. Another recent development is the application of self-consistent models [29.8] to describe the deformation behavior of polycrystals, without the assumptions made by the classical models of Taylor and Sachs [29.7]

29.2 Previous Work

Samples of four cast Al-Cu alloys with the compositions provided in Table 1 were obtained. The following experiments have been performed:

- TEM and scanning electron microscopy (SEM) of microstructures in the as-cast, aged, and overaged conditions;
- Creep testing at 300°C and 350°C, as well as qualification of rate-limiting creep mechanisms, and modeling of creep rates at each temperature;
- Time-of-flight, *in situ* neutron diffraction during tension and creep at various temperatures and aging conditions to study changes in dominant deformation mechanisms during strain hardening.

29.3 Recent Progress

29.3.1 Publicity

The General User Proposal entitled “Three- and Four-Dimensional Characterization of Precipitate Evolution in Al-Cu and Al-Ag Alloys”, submitted to Argonne National Laboratory’s Advanced Photon Source (APS), was accepted.

Center Proprietary – Terms of CANFSA Membership Agreement Apply

Preliminary static experiments to examine precipitates in 3-D have been performed, and data anlaysis in underway. Additional beamtime has been allocated for December 2018, when additional aging conditions will be studied and *in situ* experiments of precipitate evolution may begin.

A talk entitled "Identification of Deformation Mechanisms in Cast Al-Cu Alloys via Neutron Diffraction" was presented at the TMS Annual Meeting 2018 by Milligan et al. in Spring 2018. A poster entitled "Observation and Modeling of Strain Hardening Anisotropy in Al-Cu Alloys via Neutron Diffraction" by Milligan et al. was presented at the 18th International Conference on the Strength of Materials in Summer 2018.

29.3.2 Modeling of Deformation Mechanisms

In order to simplify ongoing modeling efforts and obtain an understanding of microstructure-dependent mechanical properties, aluminum alloy 206 was first observed, since it has the best understood precipitation and mechanical behavior. Alloy 206 also has a wide range of representative microstructures that can be created, containing multiple morphologies and phases of precipitates.

The macroscopic yielding behavior of alloy 206 follows a pattern consistent with the observed microstructures (Figures 29.1 and 29.2). However, the strain hardening curves contain some interesting information. A shift from linear strain hardening to a more gradual curve suggests a change in strain hardening mechanism(s). This is due to precipitates growing and transforming from thin precipitates that are easy for dislocations to shear through to thicker precipitates that are more difficult to shear through (Figure 29.2).

The model described in [29.4] has been applied as a curve-fit utilizing the five fitting parameters within the model. Contributions from two different strain hardening mechanisms were backed out and are shown in Figure 29.3. A shift from mostly isotropic hardening (increased forest dislocation density and tangling) to a mix of isotropic and kinematic (primarily Orowan looping) mechanisms occurs, as some precipitates begin to support Orowan loops. Yet, even in the overaged conditions where precipitates have traditionally been treated as completely unshearable, there seems to be a fraction of precipitates that do not support Orowan loops. Instead, some of the precipitates undergo a process referred to as "delayed shearing", where the buildup of Orowan loops causes a large stress concentration, which collapses the Orowan loops as they shear through the precipitate and annihilate. A schematic of this process is shown in Figure 29.4.

This fraction of precipitates was discussed by da Costa Teixiera [29.3, 29.4]. From this, it is easy to assume the ability of precipitates to support Orowan loops is simply a function of precipitate thickness. This assumption is not supported by data from neutron diffraction. The strain hardening behavior appears to be highly anisotropic based on grain orientation in conditions where precipitates are semi-shearable (Figure 29.5). This suggests that precipitates are becoming shearable or non-shearable based on both orientation *and* size.

An attempt to quantify this observation based upon an energetic approach is underway. The creation of new interface when a precipitate is sheared has two components: chemical energy and strain energy. The chemical energy component is a function of precipitate size, morphology, and structure. Therefore, this component should be completely isotropic. The strain energy is a function of lattice mismatch between the precipitate and matrix, and the elastic moduli of the precipitate and matrix. Because the slip plane through the precipitate and matrix is well-defined, the direction of lattice mismatch of each shearing event will always be geometrically similar to the others, and therefore the elastic energy contribution will also be isotropic.

There is also a third contribution to the elastic strain energy component of the total interfacial energy: the applied stress effect. A well-established system where this elastic energy has a large impact on the precipitate interface morphology is Ni-based superalloys during a process called rafting [29.9]. In this, the combination of a lattice mismatch between particle and matrix, as well as a difference in their elastic moduli, preferentially create interfaces that are either normal or transverse to the tensile direction. This happens when the applied stress acts in a direction similar to the interfacial strain. The stiffer phase is affected less than the softer phase, so the interfacial strain can be counteracted by the applied stress. This effect could also be contributing to the precipitate shearing in the Al-Cu system.

To quantify this effect, the magnitude and direction of the lattice mismatch stress must be found. An illustration of this is shown in Figure 29.6. Next, the following formula was applied:

$$\Delta\gamma_{shear} \propto \sigma_{app} * \Delta Y * \delta * \sum_n \frac{(\cos(\theta) - \nu \sin(\theta))}{n} \qquad \text{[Eqn. 29.1]}$$

Center Proprietary – Terms of CANFSA Membership Agreement Apply

where $\Delta\gamma_{shear}$ is the difference in shearing energy, σ_{app} is the applied stress, ΔY is the difference in Youngs moduli between precipitate and matrix in the direction of lattice mismatch, δ is the lattice mismatch, θ is the angle between the lattice mismatch strain and the applied stress, and ν is the Poisson's ratio in the direction of the lattice mismatch. The sum is over the full multiplicity of the lattice mismatch direction and the applied stress direction. Since the precipitates are stiffer than the matrix, positive values will detract from shearability of precipitates.

This change in the energy of newly-created interface can be directly correlated to the ability of precipitates to support Orowan loops, and, in turn, the grain's ability to support kinematic strain hardening. The change in energy is compared to the average strain hardening rate between 1-4% strain in the 200°C overaged sample in Figure 29.7. As can be seen, there is a clear linear relationship between the two, providing support for this approach.

29.4 Plans for Next Reporting Period

The following items are planned for the next reporting period:

- Perform TEM on post-deformation samples to observe precipitate shearing and confirm the slip plane in θ′;
- Complete energetic analysis of applied stress effect on precipitate shearing beyond simple correlation;
- Prepare a journal article on the content of Section 29.3.2;
- Submit the journal paper entitled "The Effect of Microstructural Stability on the Creep Behavior of Cast Al-Cu Alloys at 300°C";
- Continue to perform aging studies at the Advanced Photon Source at Argonne National Laboratory.

29.5 References

[29.1] S. Roy, L.F. Allard, A. Rodriguez, W.D. Porter, A. Shyam. Comparative Evaluation of Cast Aluminum Alloys for Automotive Cylinder Heads: Part II—Mechanical and Thermal Properties, Metallurgical and Materials Transactions A 48 (2017) 2543–2562.

[29.2] S. Roy, L.F. Allard, A. Rodriguez, T.R. Watkins, A. Shyam. Comparative Evaluation of Cast Aluminum Alloys for Automotive Cylinder Heads: Part I—Microstructure Evolution, Metallurgical and Materials Transactions A 48 (2017) 2529–2542.

[29.3] J. da Costa Teixeira, D. G. Cram, L. Bourgeois, T. J. Bastow, A. J. Hill, C. R. Hutchinson. On the strengthening response of aluminum alloys containing shear-resistant plate-shaped precipitates, Acta Materialia 56 (2008) 6109-6122.

[29.4] J. da Costa Teixeira, L. Bourgeois, C. W. Sinclair, C. R. Hutchinson. The effect of shear-resistant, plate-shaped precipitates on the work hardening of Al alloys: Towards a prediction of the strength–elongation correlation, Acta Materialia 57 (2009) 6075-6089.

[29.5] C. Liu, S. K. Malladi, Q. Xu, J. Chen, F. D. Tichelaar, X. Zhuge, H. W. Zandbergen. In-situ STEM imaging of growth and phase change of individual $CuAl_X$ precipitates in Al alloy, Scientific Reports 7 (2017) 2184.

[29.6] C. S. Kaira, V. De Andrade, S. S. Singhg, C. Kanzos, A. Kirubanandham, F. De Carlo, N Chawla, Probing Novel Microstructural Evolution Mechanisms in Aluminum Alloys Using 4D Nanoscale Characterization, Advanced Materials 29 (2017) 1703482.

[29.7] G. E. Dieter. Mechanical Metallurgy, 3rd Edition, McGraw-Hill, 1988, pp. 103-240.

[29.8] J. J. Battacharyya, B. Bittmann, S. R. Agnew. The effect of precipitate-induced backstresses on plastic anisotropy: Demonstrated by modeling the behavior of aluminum alloy, 7085, International Journal of Plasticity (2018) in press.

[29.9] F. R. N. Nabarro. Rafting in Superalloys. Metallurgical and Materials Transactions A 27 (1996) 513-530.

Center Proprietary – Terms of CANFSA Membership Agreement Apply

29.6 Figures and Tables

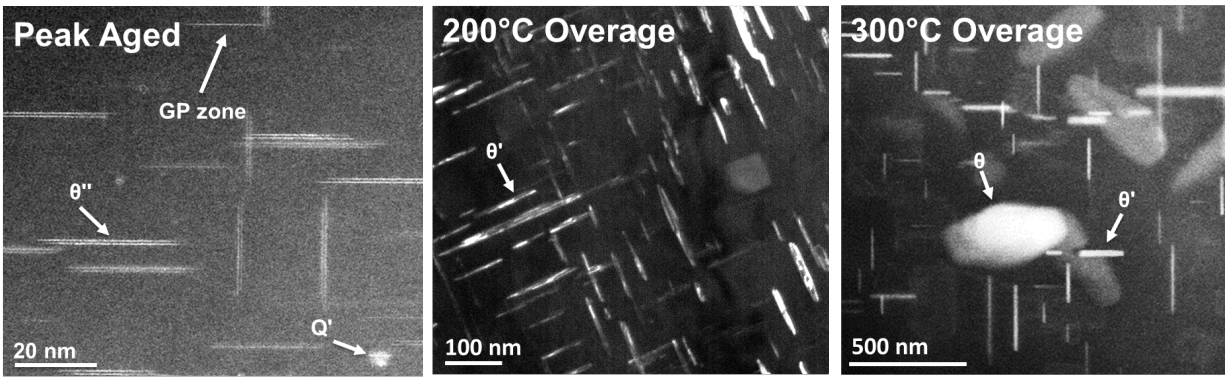

Figure 29.1: Microstructures of Al alloy 206 under various aging treatments. Overaged samples were aged at the given temperature for 200 hours. The naturally aged sample is not shown, as the nano-scale precipitates are difficult to image. TEM courtesy of L. Allard at Oak Ridge National Laboratory and F. Coury at Mines.

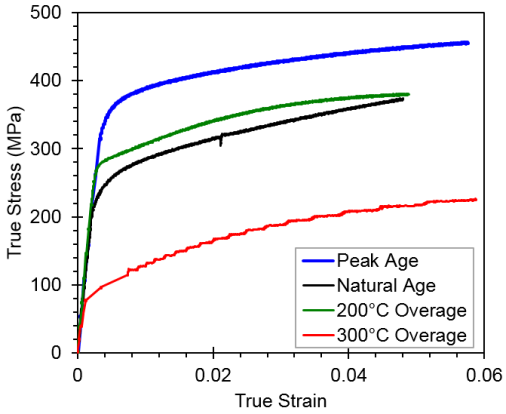

Figure 29.2: Stress-strain curve of Al alloy 206 under various after various aging treatments. Note that this stress strain behavior was studied in the neutron beam at room temperature, but was measured using a load cell and an extensometer.

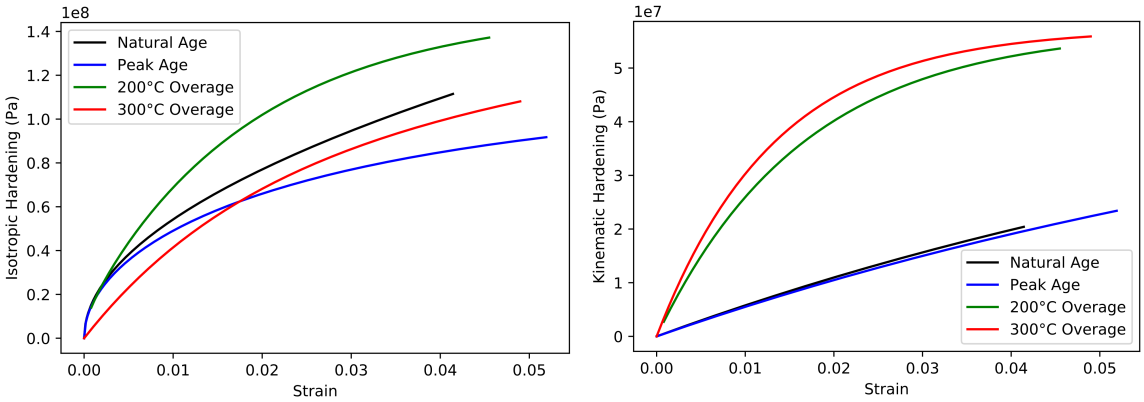

Figure 29.3: Contribution to total strain hardening from isotropic and kinematic strain hardening mechanisms. Data was backed out of the model from [29.4] after it was fit to data from Figure 29.2.

Center Proprietary – Terms of CANFSA Membership Agreement Apply

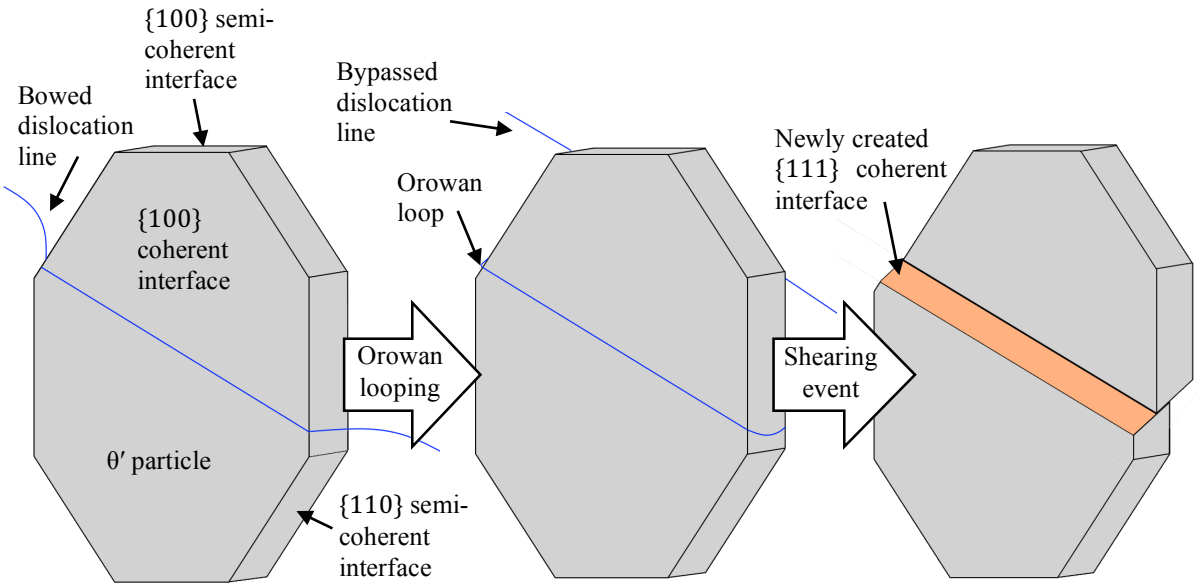

Figure 29.4: Schematic illustrating the process of delayed shearing and the creation of a new interface.

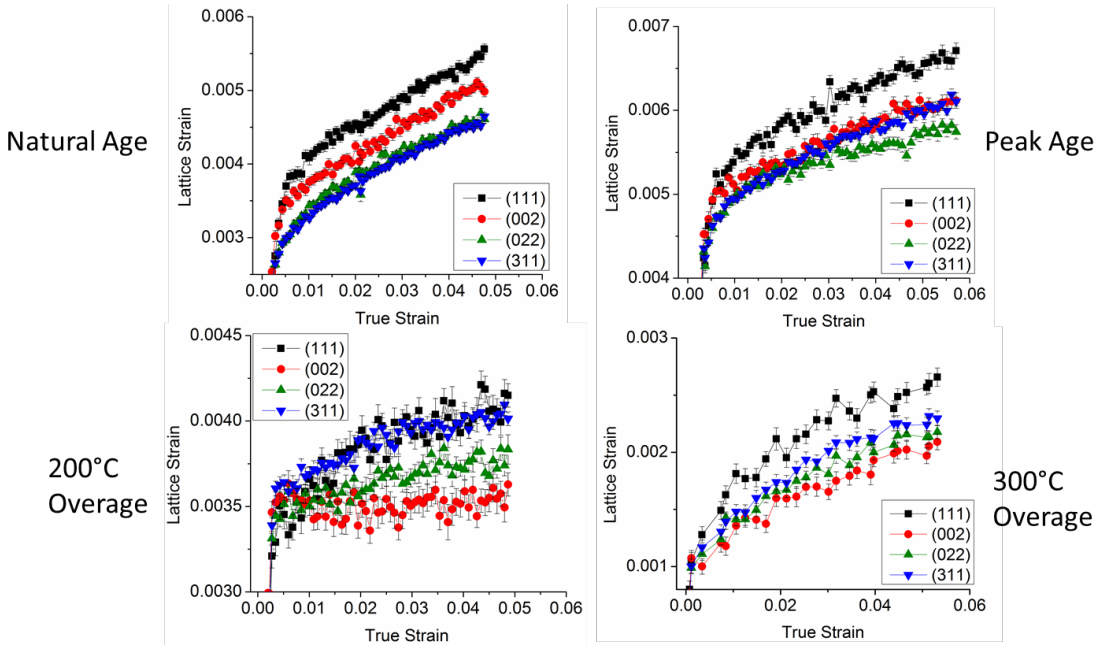

Figure 29.5: Strain hardening curves of different grain orientation families, obtained from neutron diffraction. Lattice strain (Y-axis) is proportional to internal stress.

Center Proprietary – Terms of CANFSA Membership Agreement Apply

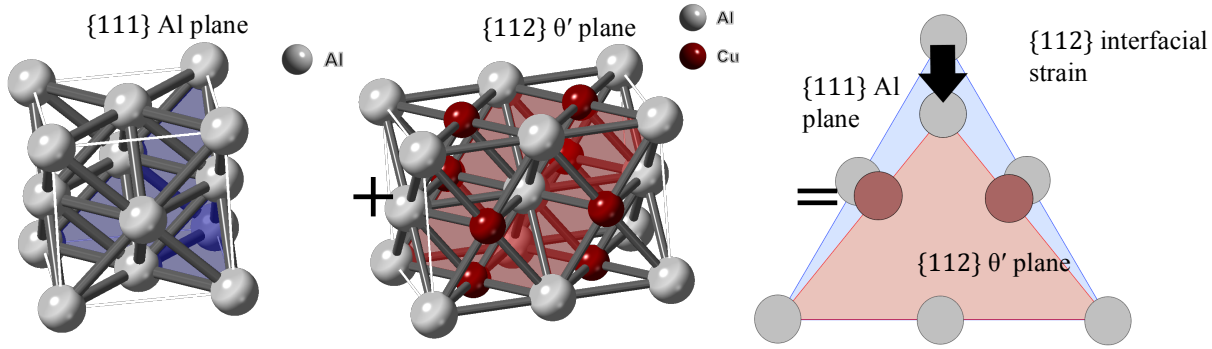

Figure 29.6: Schematic of interfacial strain in the newly-created interface illustrated in Figure 29.4.

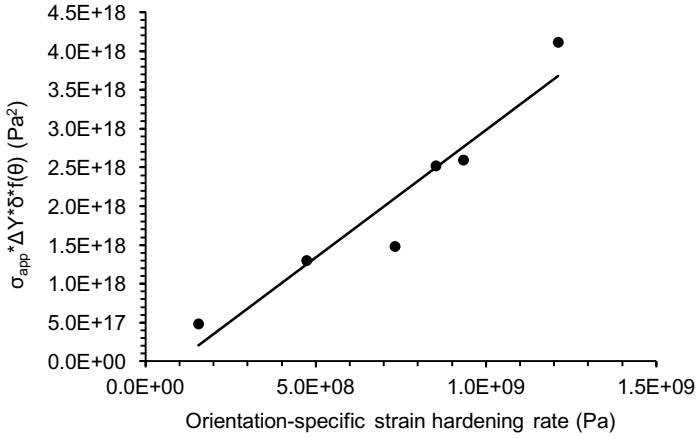

Figure 29.7: Comparison of the effect of applied stress on interfacial energy (Eq. 29.1) to the grain orientation-specific strain hardening rate in the 200°C overaged sample condition. Good correlation is taken as evidence for the importance of the applied stress effect on anisotropic strain hardening.

Table 29.1: Compositions of Al-Cu Alloys (in weight percent).

Alloy	**Si**	**Cu**	**Mg**	**Zn**	**Fe**	**Ni**	**Mn**	**Co**	**Zr**	**Ti**	**Sb**	**Cr**	**Pb**	**Al**
206-T6	0.12	4.5	0.30		0.14		0.23			0.02				bal.
319-T7	8.0	3.0	0.33	0.31	0.67	0.03	0.38			0.15		0.03	0.02	bal.
Al-7Cu-T6	0.05	6.4		0.04	0.10	0.01	0.19	<.002	0.13	0.09				bal.
RR 350-T6	0.04	4.8		0.01	0.09	1.2	0.19	0.26	0.17	0.21	0.17			bal.

Center Proprietary – Terms of CANFSA Membership Agreement Apply